Editor

GDMB
Paul-Ernst-Straße 10, D-38678 Clausthal-Zellerfeld
Internet: www.GDMB.de

Volume 1	ISBN 978-3-940276-36-0
Volume 2	ISBN 978-3-940276-37-7
Volume 3	ISBN 978-3-940276-38-4
Volume 4	**ISBN 978-3-940276-39-1**
Volume 5	ISBN 978-3-940276-40-7
Set (Volume 1+2+3+4+5)	ISBN 978-3-940276-41-4

Editorial staff:	Dipl.-Ing. Jens Harre, Ulrich Waschki
Production and marketing:	GDMB Informationsgesellschaft mbH
Printed by:	Papierflieger

© GDMB Clausthal-Zellerfeld 2011

Bibliographische Information Der Deutschen Bibliothek

Die Deutsche Bibliothek verzeichnet diese Publikation in der Deutschen Nationalbibliographie; detaillierte bibliographische Daten sind im Internet über http://dnb.ddb.de abrufbar.

Bibliographic information published by Die Deutsche Bibliothek

Die Deutsche Bibliothek lists this publication in the Deutsche Nationalbibliographie; detailed bibliographic data is available in the internet at http://dnb.ddb.de.

Proceedings

European Metallurgical Conference

EMC 2011

June 26 - 29

Düsseldorf, Germany

Volume 4

Process Metallurgy

Recycling /

Waste Treatment and Prevention

The EMC 2011-Proceedings are friendly supported by

ATLANTIC COPPER
Subsidiary of Freeport-McMoRan Copper & Gold and HATCH™

Table of Contents – Volume 4

Process Metallurgy

Recycling / Waste Treatment and Prevention

Process Metallurgy

[7] LIVAK, R.J., PAPAZIAN, J.M.: Effects of copper on precipitation and quench sensitivity of AlZnMg alloys. Scripta Metallurgica, Vol. 18, 1984, 483-488.

[8] ZHANG, K., LIU, Z., YE, Ch., XU, X., ZHENG Q.: Evolution of undissolved phases in high-zinc content super-high strength aluminum alloy during ageing. Trans. Nonferrous Met. Soc. China, Vol. 14, Nr. 2, 2004, 356-361.

[9] FERRAGUT, R., SOMOZA, A., TOLLEY, A.: Microstructural evolution of 7012 alloy during the early stages of artificial ageing. Acta Materialia, Vol. 47, Issue 17, 1999, 4355-4364.

[10] BOVARD, F.S.: Environmentally induced cracking of an Al-Zn-Mg-Cu alloy. Diploma thesis, University of Pittsburgh, 2005.

[11] STARNIK, M.J., GAO, N., FURUKAWA, M., HORITA, Z., XU, Ch., LANGDON, T.G.: Microstructural developments in a spray-cast Al-7034 alloy processed by equal-channel angular pressing. Rev. Adv. Material Science 7, 2004, 1-12.

[12] WERENSKIOLD, J.C., DESCHAMPS, A., BRÉCHET, Y.: Characterization and modeling of precipitation kinetics in an Al–Zn–Mg alloy. Materials Science and Engineering A, Vol. 293, Issues 1-2, 2000, 267-274.

[13] FERRAGUT, R., SOMOZA, A., TORRIANI, I.: Pre-precipitation study in the 7012 Al-Zn-Mg-Cu alloy by electrical resistivity. Materials Science snd Engineering A, Vol. 334, Issues 1-2, 2002, 1-5.

[14] DE HAAS, M.-J.: Grain boundary phenomend and failure of aluminium alloys. Ph.D. thesis, Rijksuniversiteit Groningen, 2002.

[15] MACCHI, C.E., SOMOZA, A., DUPASQUIER, A., POLMEAR, I.J.: Secondary precipitation in Al-Zn-Mg-(Ag) alloys. Acta Materialia, Vol. 51, Issue 17, 2003, 5151-5158.

[16] MALONEY, S.K., HONO, K., POLMEAR, I.J., RINGER, S.P.: The chemistry of precipitates in an aged Al-2.1 Zn-1.7 Mg at. % alloy. Scripta Materialia, Vol. 41, Issue 10, 1999, 1031-1038.

[17] RIONTINO, G., FERRO, G.L., LUSSANA, D., MASSAZZA, M.: The use of DSC in describing the structure evolution of an AlZnMg alloy. Journal of Thermal Analysis and Calorimetry, Vol. 82, 2005, 83-87.

[18] NICOLAS, M.: Precipitation evolution in an Al-Zn-Mg alloy during non-isothermal heat treatments and in the heat-affected zone of welded joints. Ph.D. thesis, ENSEEG – Grenoble Institute of Technology, 2002.

[19] UNGÁR, T., LENDVAI, J., KOVÁCS, I.: Metastable phase diagram of the Al-Zn-Mg alloy system in the low concentration range of Zn and Mg. Aluminium 55. Jahrgang, Vol. 10, 1979, 663-668.

[20] PARK, J.K., ARDELL, A.J.: Correlation between microstructure and calorimetric behaviour of aluminium alloy 7075 and Al-Zn-Mg in various tempers. Material Science and Engineering A, Vol. A114, 1989, 197-203.

[21] VIANA, F., PINTO, A.M.P., SANTOS, H.M.C., LOPES, A.B.: Retroregression and reageing of 7075 aluminium alloy: microstructural characterization. Journal of Materials Processing Technology, Vol. 92-93, 1999, 54-59.

[22] SCHMUCK, C., AUGER, P., DANOIX, F., BLAVETTE, D.: Quantitative analysis of GP zones formed at room temperature in a 7150 Al-based alloy. Applied Surface Science, 87-88, 1995, 228-233.

Chemical and Structural Characterization of Steelmaking Dust from Stainless Steel Production

F. Kukurugya, D. Oráč, Z. Takáčová, T. Vindt, A. Miškufová, T. Havlík

Technical University of Kosice
Faculty of Metallurgy
Dept. of Non-ferrous Metals and Waste Treatment
Letna 9, 042 00
Kosice, Slovakia

A. Kekki, J. Aromaa, O. Forsén

Aalto University
School of Science and Technology
Dept. of Material Science and Engineering
P.O. BOX 6200, 02015
Espoo, Finland

H. Makkonen

University of Oulu
Laboratory of Process Metallurgy
P.O.BOX 4300, 90014
Oulun Yliopisto, Finland

Keywords: Steelmaking dust characterization, X-ray diffraction, chemical composition

Abstract

Steelmaking dust is considered to be a hazardous by-product from steel production. Because of large heterogeneity and anisotropy of this kind of waste it is difficult to design suitable process for its recycling. The first and the most important step for recycling process design is to characterize the material from different points of view (chemical, structural, morphological composition).

The aim of this work was to characterize the steelmaking dust from Outokumpu Stainless (Tornio, Finland). Chemical analysis was carried out by Atomic absorption spectroscopy (AAS). For structural characterization the X-ray diffraction phase analysis (XRD) was used. Morphological analysis was carried out by optical microscopy and scanning electron microscopy with semi-quantitative analysis of dust particles. Besides the analysis above also density measurements, specific area measurements and granulometric analysis were carried out.

1 Introduction

Steelmaking dust is generated as by-product from steelmaking processes in amount around 10 to 20 kg per ton of produced steel [1]. Main compounds of steelmaking dust are represented by iron

oxides [2]. Due to its chemical and physical properties, steelmaking dust was categorized as hazardous waste according to the US EPA classification [3].

The increasing demand for metals has stimulated the development of new technologies worldwide to treat secondary resources like steelmaking dusts, which can present risks to the public health and/or to the environment if managed in an incorrect way [4].

The methods for steelmaking dust processing can be divided into following categories: pyrometallurgical, hydrometallurgical processes, or their combination. Hydrometallurgical processing appears to be more perspective in the future mainly from environmental and economical point of view [5, 6].

One of the major problem regarding steelmaking dusts processing is their heterogeneity in chemical and mineralogical composition. From this reason it is difficult to design "versatil" technology for their processing and every technology must be adjusted to the certain steelmaking dust. From this reason, chemical and structural characterization of steelmaking dust is a very important stage to evaluate the recycling feasibility [7].

Both chemical and mineralogical composition depends on:

- steelmaking process – Electric arc furnace (EAF), Basic oxygen furnace (BOF) a. o.
- chemical composition of raw material – steel scrap (mainly in EAF)
- type of produced steel – carbon steel (high Zn content) or stainless steel (high Cr content).

There are several papers [1, 7-9] dealing with characterization of EAF (electric arc furnace) dust from carbon steel production but only very few papers dealing with AOD (Argon Oxygen Decarburization) converter dust from stainless steel production.

According to the analysis [4] among main metals in AOD converter sludge from stainless steel production are: Fe (34.0 %), Cr (10.2 %), Ca (7 %), Mg (3.7 %), Mn (1.7 %), Si (1.7 %) and Ni (1.4 %). These metals occur mainly in the following phases: chromite $FeCr_2O_4$, magnetite Fe_3O_4, hematite Fe_2O_3 and calcite $CaCO_3$. Nickel was identified as Fe-Ni oxide or mainly in the metallic form.

The aim of this paper is to characterize steelmaking dust from stainless steel production in AOD converter. The characterization is carried out through chemical, mineralogical, morphological and granulometric analysis.

2 Experimental

2.1 Material

Two studied samples of AOD converter dust were originally produced in Outokumpu Stainless (Tornio, Finland). These samples were signed as TH1 and TH2 are described as follows: Argon Oxygen Decarburization dust 1 (TH1) and Argon Oxygen Decarburization dust 2 (TH2).

2.2 Methods

2.2.1 Elemental analysis

Both samples were submitted to chemical analysis by using of method AAS on atomic absorption spectrophotometer Varian Spectrophotometer AA20+. The results of the analysis are documented in Table 1.

Table 1: Chemical analysis of the samples

sample	content [%]								
	Zn	Fe	Ni	Cr	Mn	Pb	Cd	Ca	LOI
TH1	9.75	29.20	0.67	18.56	1.35	0.09	0.19	5.50	1.35
TH2	5.20	18.75	2.70	13.39	1.68	0.39	0.15	17.20	1.30

As can be seen from Table 1, AOD dust is characterized by high content of chromium (> 18 % in TH1). Significantly high content of chromium (over 10 %) was also observed in samples described in papers [4, 10]. The source of chromium in AOD dust is ferrochrome used as an alloy in stainless steel production [11].

2.2.2 Density

Density of samples was evaluated by pycnometer using distilled water as medium for standard method of density measurement. The results are shown in Table 2.

Table 2: Density of samples

Sample	Density [$g \cdot cm^{-3}$]
TH 1	4.3378
TH 2	4.3841

2.2.3 Granulometry

Granulometry was determined by Scanning-foto-sedimentograf, Fritsch GmbH, Analysette. Cumulative and distribution curves of particles size in individual samples are shown in Figure 1.

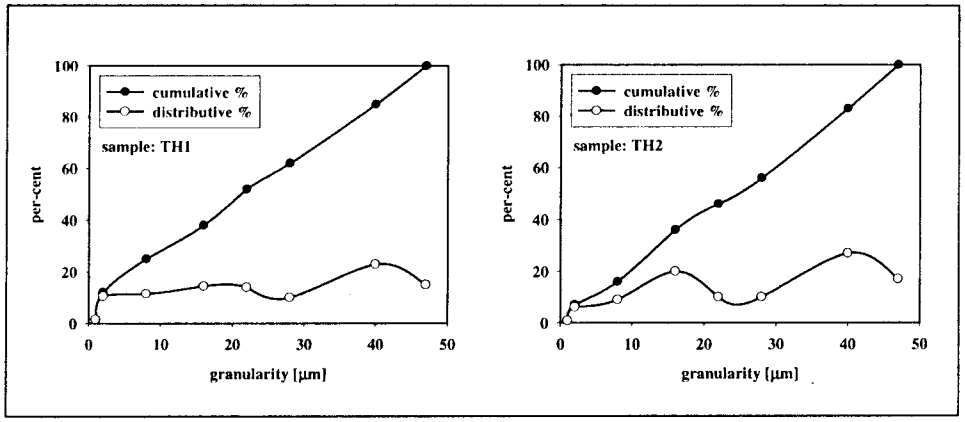

Figure 1: Granulometry of samples TH1 and TH2: Cumulative and distributive curves

The results of granulometric analysis showed that both sample have similar granulometry where 100 % of all particles is below 50 μm. From cumulative curves of samples TH1 and TH2 can be clearly seen that there are two major fractions in size range 8 to 22 μm and 28 to 47 μm, which represent 65 % in the sample TH1 and 74 % in the sample TH2.

2.2.4 Specific area

Specific area and micropores of individual samples was determined by BET method using liquid nitrogen and helium (99.9 %) as media. Used apparatus was Micromeritics' Gemini 2360 Series of surface area analyzers, Germany. The results are shown in Table 3.

Table 3: Specific area and micropores volume of samples

Sample	S_M (multi) [m^2/g]	S_A (Area) [m^2/g]	Pores volume [cm^3/g]
TH 1	3.8005	3.6172	0.0028
TH 2	3.1210	2.9630	0.0023

2.2.5 Optical microscopy

Samples were introduced to observation by optical microscopy by using Digital microscope Dino-Lite Pro AM413T. The magnification 190× was used for each sample. No optical filters were used at observation. These observations allowed not only the appreciation of macromorphology of sample constituents, but also the colour resolution, what is impossible by using of SEM microscopy.

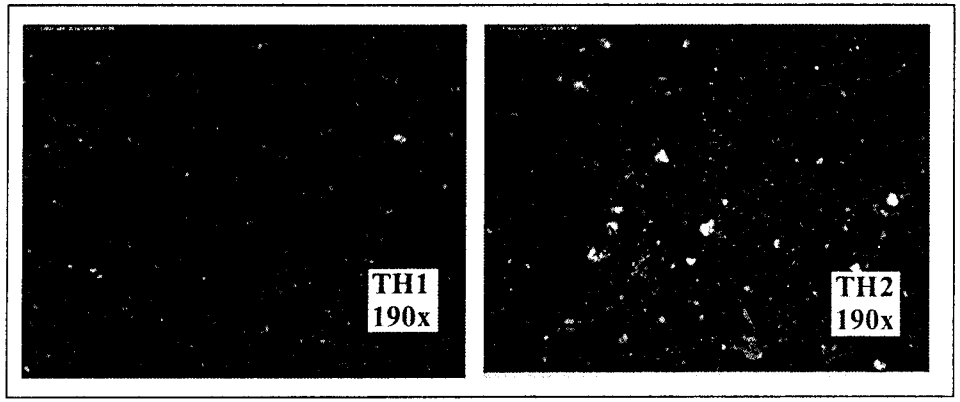

Figure 2: Morphology of AOD converter dusts – samples TH1 and TH2

As can be seen from Figure 2 particles in both samples have predominantly spherical shape where bigger particles are covered with smaller ones. The difference between both samples is small white particles present in the sample TH2. Their presence can be explained by higher content of Ca in the sample TH2 in compare with TH1 (Table 1).

2.2.6 Scanning electron microscopy

Both of morphology of samples and chemical microanalysis was determined on samples. Scanning electron microscope JEOL 5800 was used for study of morphology. Chemical microanalysis was made by Energy-Disperse Analyzer LINK 3.1 installed on scanning electron microscope JEOL 5800.

Morphology of samples – SEM - EDX

The morphology of samples is documented by Figures 3 and 4. Results of semi-quantitative analysis of dust particles are given in Tables 4 and 5.

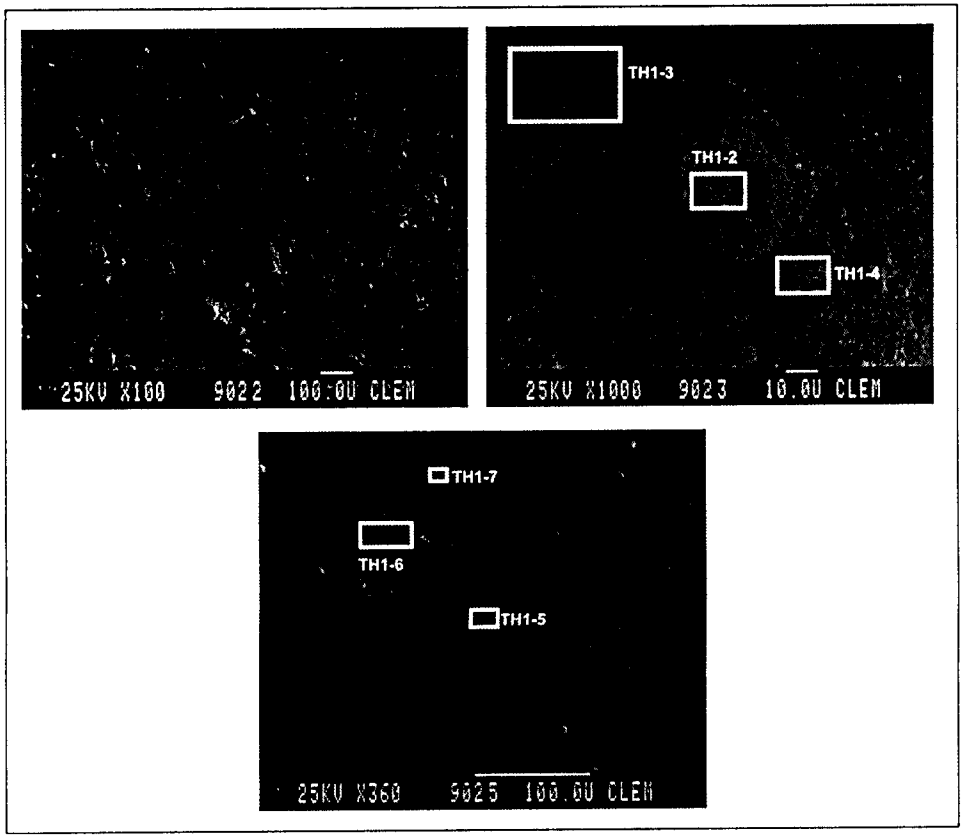

Figure 3: Morphology of dust particles TH1

Table 4: Results of semi-quantitative elemental microanalyses of sample TH1

sample	content [mass %]									
	Mg	Si	S	K	Ca	Cr	Mn	Fe	Ni	Zn
TH1-1 (background area)	2.7	2	0	1.4	10.9	11.3	4.1	46	0.7	2.7
TH1-2	1.3	1	0	0.9	1.2	20.5	5.4	62.6	1.2	2.1
TH1-3	2	1.7	0	1.6	2.8	12.2	4.4	50.7	1.1	3.1
TH1-4	1	1.2	0	1.3	36.6	9	3.7	33.7	0.5	2.1
TH1-5	1.5	0.9	0	1.5	24	10.2	3.9	39.5	0.5	2.8
TH1-6	1.7	1.4	0	2	9	12.2	4.2	48.5	0.7	2.1
TH1-7	0	0.7	0	0.2	0.4	2.7	0.9	90.4	0.2	1.6

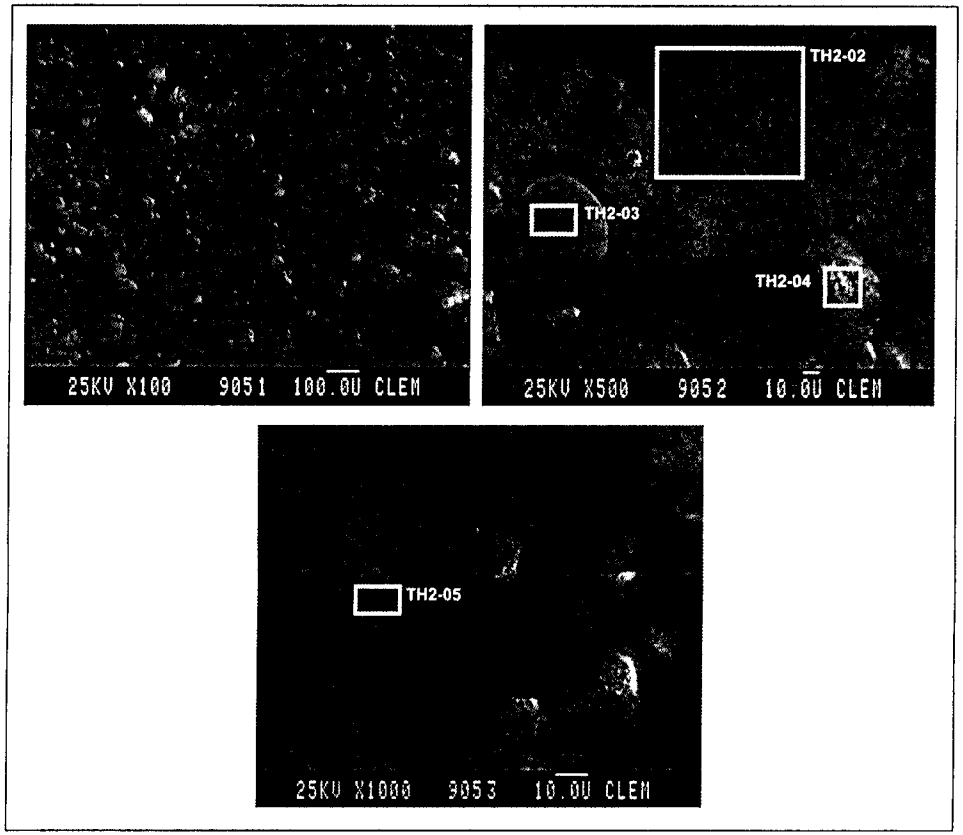

Figure 4: Morphology of dust particles TH2

Table 5: Results of semiquantitative elemental microanalyses of sample TH2

sample	content [mass %]									
	Mg	Si	S	K	Ca	Cr	Mn	Fe	Ni	Zn
TH2-01 (background area)	2.5	2.1	0	1.7	32.2	12.1	5.1	32.5	2.4	9.5
TH2-02	2.6	1.3	0	1.5	33.7	12	4.8	31.5	3	9.5
TH2-03	0.6	0.5	0	0.6	13.8	3.7	1.5	73.1	2.2	3.9
TH2-04	1.2	0.5	0.2	1.9	37.1	11.7	6.8	30.1	2.8	7.6
TH2-05	0.5	0.5	0	0.3	93.6	0.7	0.3	1.9	0	2.1

Electron probe micro-analyzer (EPMA)

TH1 and TH2 samples were also investigated by using of EPMA. Before electron probe microanalyses the samples were studied and photographed in reflecting light using a polarization microscope Olympus BX51. Microanalyses were made using JEOL JXA-8200 electron probe microanalyzer. Acceleration voltage was 15 kV and beam current 15 nA.

It follows from his observation that except of heterogeneous character of samples, phases occurring frequently are such as: silicon and ferrous silicon phases (Figure. 5a, b), Fe-Cr phases, chromite and Cr-Fe-oxide (Figure 6a, b), Magnesiochromite and glass (Figure 7a, b), Cr-Fe oxide (Figure 8a, b) and in TH2 Mo-phases (Figure 9a, b).

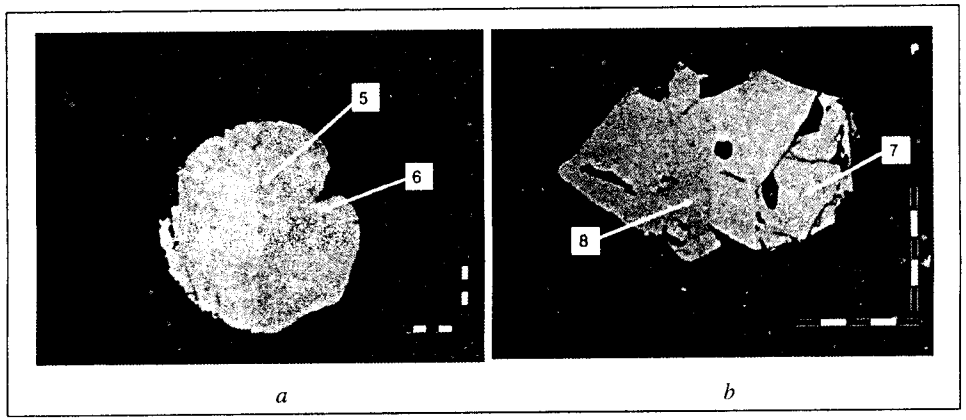

Figure 5: Silicon and ferrous silicon phases in the sample TH2

The main elements of areas 5, 6, 7 and 8 in the figure 5 are characterized by high content of Si, Fe and C. Area 5 contains 5.3 % C, 32 % Si and 58.3 % Fe. Chemical compositions in areas 6 and 7 are very similar (6 and 7.4 % C, 51 and 53 % Si, 40.2 and 37.5 % Fe). Area 8 is characterized by very high content of Si (93 %) while content of C is nearly 7 %.

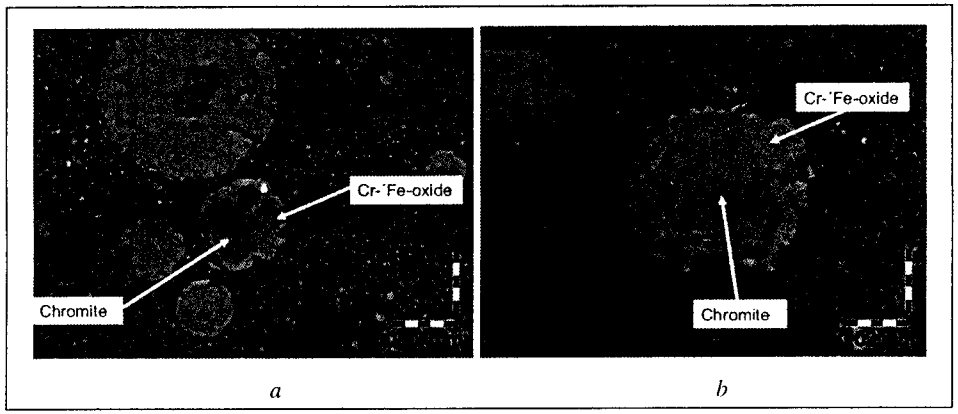

Figure 6: Chromite and Cr-Fe-oxide in the sample TH1

Phase described as *Chromite* in Figure 6a, b contains over 65 % Cr_2O_3 and 30 % FeO. On the contrary the *Cr-Fe-oxide* phase consists mainly of FeO (67 % for particle in Figure 6a and 76 % for particle in Figure 6b). Content of Cr_2O_3 in the *Cr-Fe-oxide* phase is 2.6 % in case of the particle in Figure 6a and 12 % for the particle in the Figure 6b. Both figures (Figure 6a and b) show that the phase with high Cr content is encapsulated inside the particles.

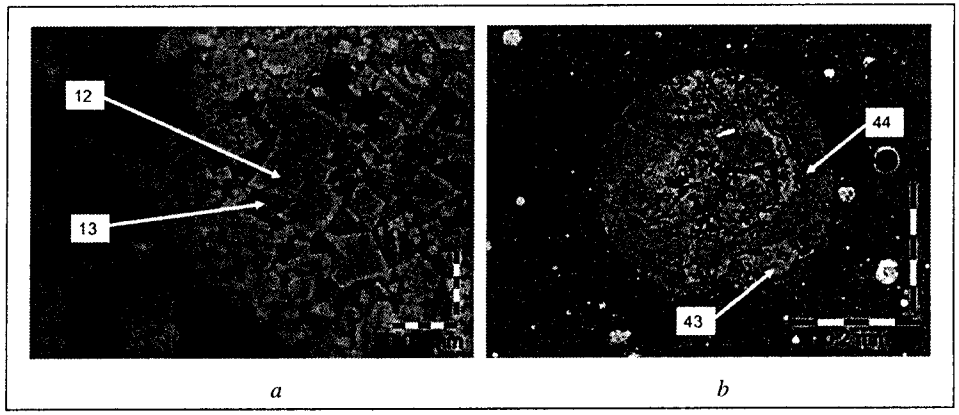

Figure 7: Magnesiochromite and glass phases in the sample TH1

Points 12 and 43 in the Figure 7 represent magnesio-chromite phase containing 17 % MgO, over 70 % Cr_2O_3 and small amount of FeO (2.5 to 4.2 %). Phase 13 is glass phase consisting of SiO_2 (17 %), CaO (32 %) and FeO (40 %). Phase 44 is a mixture of oxides such as MgO (8 %), SiO_2 (15 %), CaO (39 %), Cr_2O_3 (11 %), MnO (2 %) and FeO (17 %).

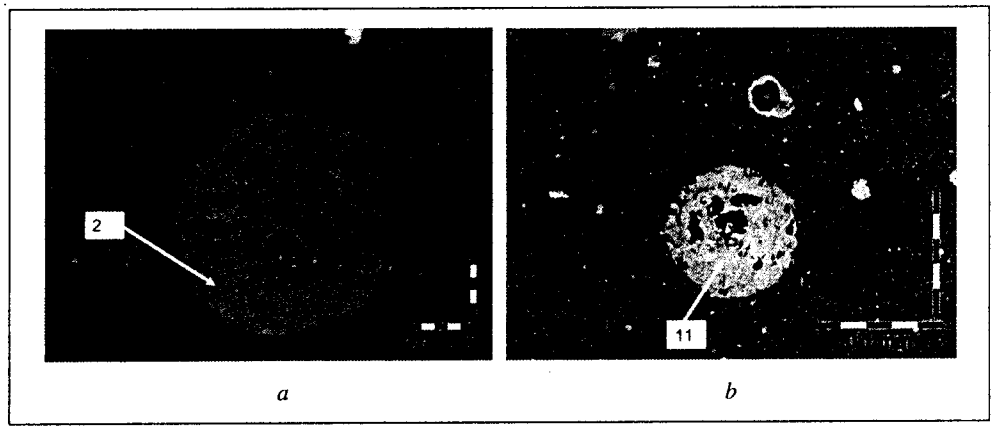

Figure 8: Cr-Fe-oxide phase in the sample TH1

Particles (2, 11) displayed in the Figure 8 consist of two oxides Cr_2O_3 and FeO. Particle 2 contains 11 % Cr_2O_3, 78 % FeO and particle 11 contains 6.5 % Cr_2O_3, 83.5 % FeO.

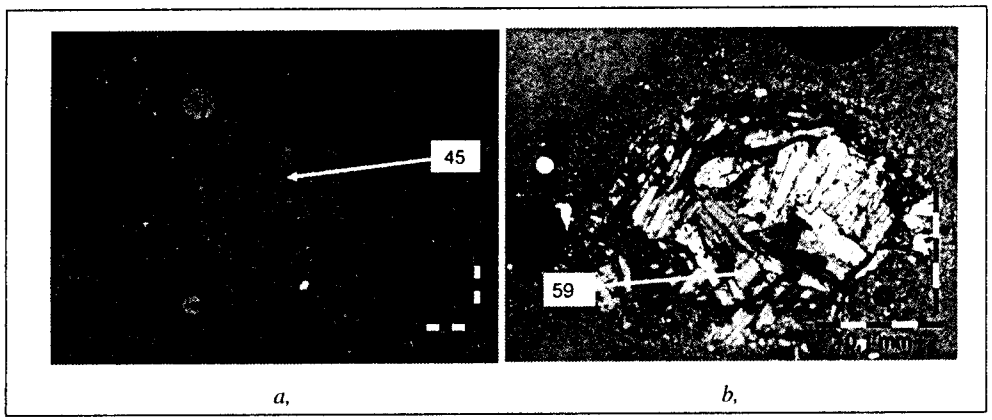

Figure 9: Mo-oxide phases in the sample TH2

Phases in Figure 9a, b (45, 59) are characteristic by high content of MoO_3. Phase marked with number 45 (Figure 9a) contains more than 54 % MoO_3 and 30 % CaO. Phase 59 (Figure 9b) contains practically only MoO_3 (over 80 %).

2.2.7 X-Ray diffraction qualitative phase analysis

X-ray diffraction qualitative phase analysis was made on the PANalytical X'Pert PRO MRD X-Ray diffractometer using Co Kα radiation. X-Ray diffraction patterns of individual samples are shown on the Figure 10 and 11, results of X-Ray diffraction qualitative phase analysis made by computer system RIFRAN are given in Table 6 and 7.

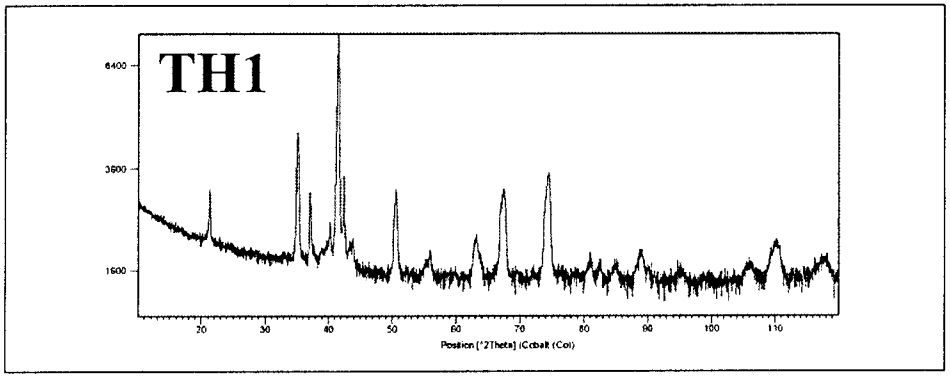

Figure 10: XRD pattern of the sample TH1

Table 6: Identified phases in the sample TH1

Ref. Code	Compound Name	Chemical Formula
01-089-2618	Iron Chromium Oxide	$FeCr_2O_4$
01-070-2551	Zinc Oxide	ZnO
01-086-1350	Iron Oxide	$Fe_{2.937}O_4$
01-082-1532	Zinc Chromium Oxide	$(Zn_{0.982}Cr_{0.018})(Cr_{1.982}Zn_{0.018})O_4$
01-089-2779	Calcium Hydroxide	$Ca(OH)_2$

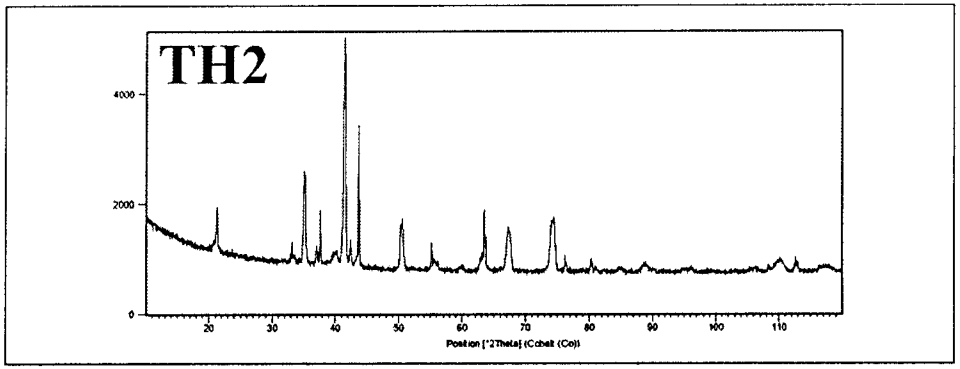

Figure 11: XRD pattern of the sample TH2

Table 7: Phases identified in the sample TH2

Ref. Code	Compound Name	Chemical Formula
01-070-4068	Calcium Oxide	CaO
01-089-6228	Iron Silicon Oxide	$(Fe_{0.769}Si_{0.231})(Fe_{0.975}Si_{0.025})_2O_4$
00-048-1066	Zinc Hydroxide	$Zn(OH)_2$
01-086-1357	Iron Oxide	$Fe_{2.950}O_4$
01-081-2041	Calcium Hydroxide	$Ca(OH)_2$
00-004-0759	Iron Chromium Oxide	$Fe_2Cr_2O_4$

3 Conclusions

Two samples of AOD converter dust from stainless steel production were from both elemental as well as mineralogical composition point of view investigated in this paper. The samples were delivered from Outokumpu Stainless (Tornio, Finland).

The following methods for analyzing were used: elemental analysis, density measurements, specific area measurements, optical microscopy, scanning electron microscopy and X-Ray diffraction qualitative phase analysis.

Elemental analysis shows that the main metals in both samples were Fe, Cr, and Zn whereby the content of Cr in sample TH2 was more than 18 %.

Granulometric analysis showed heterogeneity of size distribution for both sample TH1 and TH2 where 100 % of all particles were below 50 µm. Two main size fraction +8-22 µm and +28-47 µm represent over 60 % of all particles in the sample TH1 and 74 % in the sample TH2.

XRD diffraction analysis detected as main phases in both samples: chromite $FeCr_2O_4$ and magnetite Fe_3O_4. As it was demonstrated by elemental analysis (Table 1) sample TH2 is characteristic by high content of Ca which is most likely present as calcium oxide CaO and/or calcium hydroxide $Ca(OH)_2$. Zinc is probably present as zinc hydroxide $Zn(OH)_2$ and zinc oxide ZnO. It is necessary to consider that both samples (TH1 and TH2) contain ferritic phases having very similar XRD patterns what makes their exact identification problematic. Moreover, some minerals are encapsulated inside of grains. These are not identified by XRD phase analysis as "invisible" for X-rays.

Electron probe micro-analysis showed that in both samples are areas with high content of the following metals: Cr, Mg, Ca (Figure 7), Fe (Figure 8), Si (Figure 5), and Mo (Figure 9). It was also observed that many of the mentioned metals are encapsulated inside particles what can cause problems during recycling process, especially during hydrometallurgical processes. In addition, Cr and Fe were found mainly in the form of ferrites, which are very resistant to hydrometallurgical processing.

Acknowledgement

This work was supported by Ministry of Education of the Slovak republic under grant MŠ SR 1/0123/11. This contribution is also the result of the project implementation Research excellence centre on earth sources, extraction and treatment supported by the Research & Development Operational Programme funded by the ERDF, ITMS number: 26220120017. This work has been done in the METDUST project of the ELEMET research program funded by FIMECC Oy. The financial support of TEKES, Outokumpu Oyj, Outotec Oyj and New Boliden Oyj (Kokkola) is gratefully acknowledged.

References

[1] LAFOREST, G. & DUCHESNE, J. (2006): Characterization and leachability of electric arc furnace dust made from remelting of stainless steel – Journal of Hazardous Material B135: 156-164.

[2] MARTINS, F. M., NETO, J. M. R. & CUNHA, C.J. (2008): Mineral phases of weathered and recent electric arc furnace – Journal of Hazardous Materials 154: 417-425.

[3] UNITED STATES ENVIRONMENTAL PROTECTION AGENCY (2009): Assessing the management of lead in scrap metal and electric arc furnace dust – Final Report, EPA530-R-09-004.

[4] MAJUSTE, D. & MANSUR, M. B. (2008): Characterization of the fine fraction of the argon oxygen decarburization with lance (AOD-L) sludge generated by the stainless steelmaking industry – Journal of Hazardous Materials 153: 89-95.

[5] HAVLÍK, T., SOUZA, B.V., BERNARDES, I.A.H., SCHNEIDER, A.M. & MIŠKUFOVÁ, A. (2006): Hydrometallurgical processing of carbon steel EAF dust – Journal of Hazardous Materials B135: 311–318.

[6] OUSTADAKIS, P., TSAKIRIDIS, P .E., KATSIAPI, A. & AGATZINI-LEONARDOU.S. (2010): Hydrometallurgical process for zinc recovery from electric arc furnace dust (EAFD), Part I: Characterization and leaching by diluted sulphuric acid – Journal of Hazardous Materials 179:1-7.

[7] MACHADO, J. G. M. S., BREHM, F.A., MORAES, C.A. M., SANTOS, C. A., VILELA, A. C. F. & CUNHA, J. B. M. (2006): Chemical, physical, structural and morphological characterization of the electric arc furnace dust – Journal of Hazardous Materials B136: 953-960.

[8] MANTOVANI, M. C., TAKANO, C. & BÜCHLER, P. M. (2004): EAF and secondary dust characterisation – Iron and Steelmaking, Vol. 31, No. 4 : 325-332.

[9] ANTREKOWITSCH, J. & GRIESSACHER, T. (2008): Characterization of zinc containing residues from metallurgical processes – REWAS 2008: 775-783.

[10] TANG, M., PENG, J., PENG, B., YU, D. & TANG C. (2008): Thermal solidification of stainless steelmaking dust- Trans. Nonferrous Met. Soc. China 18: 202-206.

[11] MUKHERJEE, A.B.(1998): Chromium in the environment of Finland – The Science of the Total Environment 217: 9-19.